J Neurophysiol 112: 1491–1504, 2014.
First published July 9, 2014; doi:10.1152/jn.00437.2014.

Intrinsic bursting of AII amacrine cells underlies oscillations in the rd1 mouse retina

Hannah Choi,[1] Lei Zhang,[2] Mark S. Cembrowski,[3] Carl F. Sabottke,[2] Alexander L. Markowitz,[2] Daniel A. Butts,[2] William L. Kath,[1] Joshua H. Singer,[2] and Hermann Riecke[1]

[1]*Department of Engineering Sciences and Applied Mathematics, Northwestern University, Evanston, Illinois;* [2]*Department of Biology, University of Maryland, College Park, Maryland; and* [3]*Howard Hughes Medical Institute, Janelia Farm Research Campus, Ashburn, Virginia*

Submitted 11 June 2014; accepted in final form 26 June 2014

Choi H, Zhang L, Cembrowski MS, Sabottke CF, Markowitz AL, Butts DA, Kath WL, Singer JH, Riecke H. Intrinsic bursting of AII amacrine cells underlies oscillations in the rd1 mouse retina. *J Neurophysiol* 112: 1491–1504, 2014. First published July 9, 2014; doi:10.1152/jn.00437.2014.—In many forms of retinal degeneration, photoreceptors die but inner retinal circuits remain intact. In the rd1 mouse, an established model for blinding retinal diseases, spontaneous activity in the coupled network of AII amacrine and ON cone bipolar cells leads to rhythmic bursting of ganglion cells. Since such activity could impair retinal and/or cortical responses to restored photoreceptor function, understanding its nature is important for developing treatments of retinal pathologies. Here we analyzed a compartmental model of the wild-type mouse AII amacrine cell to predict that the cell's intrinsic membrane properties, specifically, interacting fast Na and slow, M-type K conductances, would allow its membrane potential to oscillate when light-evoked excitatory synaptic inputs were withdrawn following photoreceptor degeneration. We tested and confirmed this hypothesis experimentally by recording from AIIs in a slice preparation of rd1 retina. Additionally, recordings from ganglion cells in a whole mount preparation of rd1 retina demonstrated that activity in AIIs was propagated unchanged to elicit bursts of action potentials in ganglion cells. We conclude that oscillations are not an emergent property of a degenerated retinal network. Rather, they arise largely from the intrinsic properties of a single retinal interneuron, the AII amacrine cell.

AII amacrine cell; bursting; oscillation; retinal degeneration

RETINITIS PIGMENTOSA (RP) refers to a collection of retinal diseases in which photoreceptors die (rods followed by cones) (Adams et al. 2007; Hartong et al. 2006). Mutations in the β-subunit of rod cGMP-phosphodiesterase occur both in human RP and in mouse models of the disease (Chang et al. 2002, 2007; Hartong et al. 2006). The rd1 mouse is an established model of RP specifically and of blinding retinal disorders generally (Carter-Dawson et al. 1978; Jimenez et al. 1996).

Ganglion cells in rd1 retinas are driven to fire bursts of action potentials by phasic synaptic inputs arriving at ~10 Hz (Marc et al. 2007; Margolis et al. 2008; Stasheff 2008). Because oscillatory activity might inhibit normal retinal responses to restored photoreceptor function or might inhibit cortical responses to restored visual input by inducing maladaptive changes in visual circuits, interest in elucidating the circuitry generating it has grown. Speaking to the importance of understanding circuit changes following vision loss, restoration of photoresponsiveness in a blind human patient did not restore visual perception (Fine et al. 2003).

The synaptic drive underlying ganglion cell bursting likely originates in the network of electrically coupled AII amacrine cells and ON cone bipolar (ONCB) cells (Borowska et al. 2011; Trenholm et al. 2012). This notion is supported by the observation that bursting in ON and OFF alpha ganglion cells is anticorrelated (Margolis et al. 2014), just as light-evoked synaptic excitation to these cell types in the normal retina is anticorrelated (Murphy and Rieke 2006); the AII network generates this anticorrelation by providing simultaneously indirect excitation to ON alpha cells and direct inhibition to OFF alpha cells (Demb and Singer 2012).

Here, we demonstrate that oscillations in the rd1 retina arise from intrinsic membrane properties of AIIs; they are not an emergent property of a network of coupled neurons with heterogeneous intrinsic electrical properties, as has been suggested (Trenholm et al. 2012). Specifically, we tested the hypothesis that AIIs in the rd1 retina are hyperpolarized relative to their wild-type counterparts and that this hyperpolarization permits an interaction between a fast, depolarizing Na conductance and a slow, hyperpolarizing, M-type K conductance to generate phasic bursting, just as it does in the wild-type retina (Cembrowski et al. 2012).

A model of the AII (Cembrowski et al. 2012) allowed us to predict effects of M-type K current activators and inhibitors on oscillations observed experimentally during whole cell recordings from AIIs in a retinal slice preparation. Pharmacologically induced alterations in AII activities were propagated unchanged to ganglion cells, as revealed by whole cell recordings from individual cells and by multielectrode array recordings of population activity. We conclude that the intrinsic properties of rd1 and wild-type AIIs need not differ; rather, hyperpolarization arising from reduced light-dependent synaptic input is sufficient to unmask bursting. Electrical coupling is relevant only because it affects the AII hyperpolarization. Our finding indicates that treatment of retinal degeneration might benefit from preventing hyperpolarization of AIIs. Inducing light sensitivity in ON bipolar cells (see Lagali et al. 2008) may accomplish this.

MATERIALS AND METHODS

Electrical recordings from in vitro retinal preparations. C3HeJ mice (*rd-1/rd-1*; RD1), which carry a mutation in the *Pde6b* gene encoding the β-subunit of cGMP-phosphodiesterase and lose the outer nuclear layer by 4 wk of age, were obtained from the Jackson

Address for reprint requests and other correspondence: H. Riecke, Dept. of Engineering Sciences and Applied Mathematics, Northwestern Univ., Evanston, IL 60208 (e-mail: h-riecke@northwestern.edu).

Laboratories (Bar Harbor, ME) and killed at postnatal *days 40-50*, when their retinas were not responsive to light due to the loss of photoreceptors. Mice were anesthetized by isofluorane inhalation and decapitated before enucleation, as approved by the Animal Care and Use Committee at the University of Maryland. Retinas were isolated into cooled (~15°C) bicarbonate-buffered Ames' medium (Sigma) equilibrated with 95% O_2-5% CO_2 (Carbogen). Whole cell recordings were made from AII amacrine cells in retinal slices and from ganglion cells in retinal whole mount preparations (e.g., Margolis et al. 2014).

For retinal slice preparation, retinas then were embedded in low-melting temperature agarose (Sigma type VIIA, 3% in a HEPES-buffered saline), and slices (300 μm) were cut on a vibrating microtome (Leica). Slices were stored in Carbogen-bubbled Ames' medium at room temperature until use. For retinal whole mount preparation, a ~2-mm square of retinal tissue was mounted flat, photoreceptor-side down, onto Anodisc filter paper (Whatman, Florham Park, NJ). Both retinal slices and whole mounts were placed in a recording chamber mounted below an upright video-microscope (Zeiss) so that cells of interest could be visualized and targeted for whole cell recordings with pipettes containing the following (in mM): 95 K gluconate, 15 KCl, 5 NaCl, 10 HEPES, 0.2 EGTA, 8 Tris-phosphocreatine, 4 MgATP, and 0.4 NaGTP. For ganglion cells, alpha cells were targeted based on soma size (diameter 18–25 mm). Access resistances were <25 MΩ and were not compensated. For extracellular recording of ganglion cell spiking, a ~2-mm square of retinal tissue was mounted flat, ganglion cell-side down, onto a 60-channel multielectrode array (MEA; square array; 30-μm electrodes with 200-μm spacing; Multichannel Systems).

In all cases, during recordings, the tissues were super-fused with Ames' medium (~34°C) to which drugs were added as noted. Picrotoxin (100 μM), strychnine (0.5 μM), dinitroquinoxaline-2,3-dione (DNQX; 25 μM), and APV (50 μM) were added to block $GABA_A$ receptor-, glycine receptor-, AMPA/kainate receptor-, and NMDA receptor-mediated currents, respectively. L-(+)-2-amino-4-phosphonobutyric acid (L-AP4; 2–10 μM) was added to activate mGluR6 receptors on ON bipolar cells. Tetrodotoxin (TTX; 0.5 μM) was added to block voltage-gated Na channel-mediated currents, linopiridine hydrochloride (LP; 30 μM) was added to block M-type K currents, flupiritine maleate (flu; 10 μM) was added to potentiate M-type K currents, meclofenamic acid (MFA; 100 μM) was added to block gap junctions, and $CdCl_2$ (100 μM) and $NiCl^{2+}$ (50 μM) were added to block voltage-dependent Ca currents.

Whole cell recordings were made using a MultiClamp 700B amplifier, and data were acquired using an ITC18 amplifier controlled by IgorPro (Wavemetrics). Multielectrode recordings were made using a MEA workstation (MEA-1060; Multichannel Systems), and data were acquired using MC_Rack software (Multichannel Systems).

Spike sorting of multielectrode recordings. Each electrode recording was band-pass filtered between 300 and 6,000 Hz with a four-pole Butterworth filter. Spike waveforms were then extracted using a threshold proportional to the median of the absolute value of the filtered electrode data (Quiroga et al. 2004). Putative spike waveforms were mapped into a 14-dimensional feature space defined by the first 10 principal components, the waveform peaks, the waveform troughs, the waveform energy, and the energy of the spike waveform first derivatives. Clustering in these spaces was performed using Gaussian mixture models. Single units matching the bursting characteristics of the intracellular data were included in the analysis only if the cluster had an isolation distance >3, an L ratio <3, and a Dunn index >50 (Harris et al. 2001; Schmitzer-Torbert and Redish 2004; Schmitzer-Torbert et al. 2005). Across trials in four different rd1 mouse retinas, we isolated 61 single units during exposure to L-AP4, 18 single units during exposure to LP, and 34 single units during the washout condition. The average L ratio score for these 113 single units was 0.21 ± 0.55, and the average isolation distance score was 26.98 ± 34.

Computational model. All numerical simulations were performed with MATLAB. The code is available at http://senselab.med.yale.edu/modeldb/. For the AII we used the three-compartment model from Cembrowski et al. (2012), which behaves similarly to a morphologically realistic model as shown in our previous study (Cembrowski et al. 2012) (see Fig. 4, *Ai* and *Aii*). The morphologically detailed model was built based on an AII filled with a fluorescent tracer (see Fig. 4*Ai*). Na, A-type K, and slowly activating M-type K conductances were inserted into the distal varicosity; the long neurite and the soma were taken to be passive, and the rest of the cell had a low-density A-type K conductance (Cembrowski et al. 2012). The previous study has shown that, in the morphologically detailed model, voltage responses to a brief current injection at the distal varicosity were very similar when measured in the soma, the lobules at the end of the primary denrite, and the arboreal dendrite (Cembrowski et al. 2012). Thus, excepting the distal varicosity that was shown to be the spike-initiation site (Cembrowski et al. 2012) and the attached long neurite, when spiking the rest of the AII behaves as if it is electrotonically compact. This justifies treating the soma and arboreal dendrite as a single compartment.

Specifically, our AII model consisted of a large compartment (length = 25 μm, diameter = 25 μm) representing the soma and arboreal dendrite of the AII, a thin cable-like compartment (length = 32 μm, diameter = 0.3 μm) that represents the long neurite branching from the primary dendrite, and the small initiation site (length = 2 μm, diameter = 2 μm; see Fig. 4*Aii*). For convenience, we will call the large compartment the "soma," the thin cable compartment the "cable," and the small varicosity compartment the "initiation site." Unlike in Cembrowski et al. (2012), here we treated the cable as 1 compartment instead of 11 compartments, after confirming that this change does not make a significant difference. In all three compartments, there was a passive leak conductance, with membrane resistivity of 40,000 Ω·cm^2. The specific membrane capacitance and axial resistivity were 1 μF/cm^2 and 150 Ω/cm respectively. In addition, the initiation site had a fast Na conductance ($\bar{g}_{IS,Na}$ = 0.2 S/cm^2), an incompletely inactivating A-type K conductance ($\bar{g}_{IS,A}$ = 0.08 S/cm^2), and a slow noninactivating M-type K conductance ($\bar{g}_{IS,M}$ = 0.03 S/cm^2), as this single distal initiation site has been shown to be the site of spike generation as well as of its slow modulation (Cembrowski et al. 2012). Although the soma itself was found to be passive (Tian et al. 2010), since the somatic compartment of the three-compartment model was taken to include arboreal dendrites, an A-type K conductance was included in this compartment ($\bar{g}_{IS,A}$ = 0.004 S/cm^2). These active conductances, with the reversal potentials E_{Na} = 50 mV and E_K = −77 mV, had the following kinetics.

The Na current was given by

$$i_{Na} = \bar{g}_{Na} m_{Na}^3 h_{Na} (V - E_{Na}) \quad (1)$$

where the activation variable and the inactivation variable were governed by

$$\tau_{m_{Na}} \frac{dm_{Na}}{dt} = m_{\infty,Na} - m_{Na}, \quad (2)$$

$$\tau_{h_{Na}} \frac{dh_{Na}}{dt} = h_{\infty,Na} - h_{Na}, \quad (3)$$

with

$$m_{\infty,Na}(V) = \left[1 + \exp\left(-\frac{(V - V_{1/2,m_{Na}})}{k_{m_{Na}}}\right)\right]^{-1}, \quad V_{1/2,m_{Na}} = -48 \text{ mV}, k_{m_{Na}} = 5 \text{ mV} \quad (4)$$

$$h_{\infty,Na}(V) = \left[1 + \exp\left(\frac{(V - V_{1/2,h_{Na}})}{k_{h_{Na}}}\right)\right]^{-1}, \quad V_{1/2,h_{Na}} = -49.5 \text{ mV}, k_{h_{Na}} = 2 \text{ mV}. \quad (5)$$

Both activation and inactivation of the Na current were fast, with time constants $\tau_{m_{Na}}$ = 0.01ms and $\tau_{h_{Na}}$ = 0.5ms, respectively.

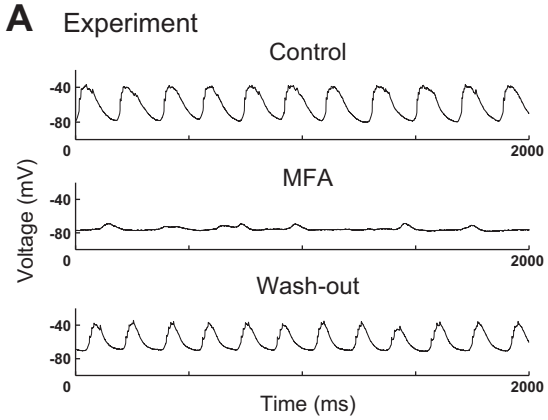

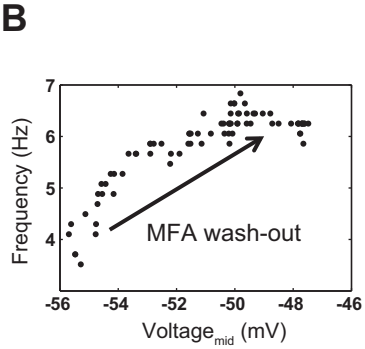

Fig. 1. Meclofenamic acid (MFA) blocks oscillations following frequency decrease and hyperpolarization of AIIs. Experiment during MFA washin and washout on an rd1 AII. *A*: representative recording of an rd1 AII shows that MFA eliminates the oscillations. The oscillation that was suppressed by MFA was restored with its frequency slowly increasing during the washout. *B*: frequency averaged over each 5-s-long sweep is plotted as a function of the midpoint membrane potential of the AII during the MFA washout.

The M-type K current was given by

$$i_{\mathrm{M}} = \bar{g}_{\mathrm{M}} m_{\mathrm{M}} (V - E_{\mathrm{K}}) \quad (6)$$

where the activation variable was described as

$$\tau_{m_{\mathrm{M}}} \frac{dm_{\mathrm{M}}}{dt} = m_{\infty,\mathrm{M}} - m_{\mathrm{M}} \quad (7)$$

with

$$m_{\infty,\mathrm{M}}(V) = \left[1 + \exp\left(-\frac{(V - V_{1/2,m_{\mathrm{M}}})}{k_{m_{\mathrm{M}}}}\right)\right]^{-1}, \quad V_{1/2,m_{\mathrm{M}}} = -40 \text{ mV}, k_{m_{\mathrm{M}}} = 4 \text{ mV}. \quad (8)$$

The M-type K current is noninactivating and activates slowly with a time constant $\tau_{m_{\mathrm{M}}} = 50$ ms.

Finally, the A-type K current was given by

$$i_{\mathrm{A}} = \bar{g}_{\mathrm{A}} m_{\mathrm{A}} \left[c h_{\mathrm{A}}^{(1)} + (1 - c) h_{\mathrm{A}}^{(2)}\right](V - E_{\mathrm{K}}), \quad (9)$$

$$c = \left[1 + \exp\left(-\frac{(V + 45)}{15}\right)\right]^{-1}, \quad (10)$$

where the activation and inactivation variables were governed by

$$\tau_{m_{\mathrm{A}}} \frac{dm_{\mathrm{A}}}{dt} = m_{\infty,\mathrm{A}} - m_{\mathrm{A}}, \quad (11)$$

$$\tau_{h_{\mathrm{A}}^{(1)}} \frac{dh_{\mathrm{A}}^{(1)}}{dt} = h_{\infty,\mathrm{A}} - h_{\mathrm{A}}^{(1)}, \quad (12)$$

$$\tau_{h_{\mathrm{A}}^{(2)}} \frac{dh_{\mathrm{A}}^{(2)}}{dt} = h_{\infty,\mathrm{A}} - h_{\mathrm{A}}^{(2)}, \quad (13)$$

with

$$m_{\infty,\mathrm{A}}(V) = \left[1 + \exp\left(-\frac{(V - V_{1/2,m_{\mathrm{A}}})}{k_{m_{\mathrm{A}}}}\right)\right]^{-1}, \quad V_{1/2,m_{\mathrm{A}}} = -10 \text{ mV}, k_{m_{\mathrm{A}}} = 7 \text{ mV}, \quad (14)$$

$$h_{\infty,\mathrm{A}}(V) = f\left[1 + \exp\left(\frac{(V - V_{1/2,h_{\mathrm{A}}})}{k_{h_{\mathrm{A}}}}\right)\right]^{-1} + (1 - f), \quad V_{1/2,h_{\mathrm{A}}} = -40.5 \text{ mV}, k_{h_{\mathrm{A}}} = 2 \text{ mV}, f = 0.83. \quad (15)$$

The A-type K current had a relatively fast activation with $\tau_{m_{\mathrm{A}}} = 1$ ms along with a fast inactivation $h_{\mathrm{A}}^{(1)}$ and a slow inactivation $h_{\mathrm{A}}^{(2)}$. Inactivation was incomplete as captured by f in the steady-state expression above, with time scales

$$\tau_{h_{\mathrm{A}}^{(1)}}(V) = 25 - 20\left[1 + \exp\left(-\frac{(V + 35)}{6}\right)\right]^{-1}, \quad (16)$$

$$\tau_{h_{\mathrm{A}}^{(2)}}(V) = \min\left\{\frac{(V + 17)^2}{4} + 26, 100\right\}. \quad (17)$$

The parameters for the A-type K conductance were well constrained by voltage-clamp recordings (Tian et al. 2010), while other parameters were fit to reproduce the experimentally observed spikelets and bursts in wild-type AIIs (Cembrowski et al. 2012). In this three-compartment AII model, we omitted an L-type Ca conductance that is present in AII cells (Habermann et al. 2003) since it was not needed to reproduce realistic AII responses in the regime of interest. For the first set of simulations (see Fig. 4), the model consisted of this three-compartmental AII in isolation, showing that a single AII is capable of generating tonic spiking and bursting. We adjusted the leak reversal potentials of the AII to reproduce the experimentally recorded membrane potentials for the wild-type and rd1 AII. We used the leak reversal potential of −10 mV to put the AII in the tonic spiking

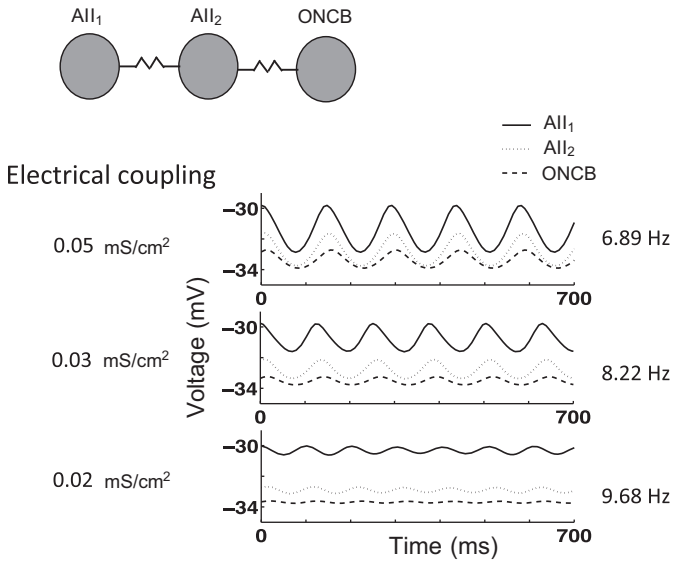

Fig. 2. A model based on gap junctions between heterogeneous AIIs does not explain the MFA-induced frequency decrease. The model in Trenholm et al. (2012), which designates the gap-junction coupled network of heterogeneous AIIs as the key to the rd1 oscillations, does not explain the experimental observed frequency decrease under MFA application. The model consists of 2 slightly heterogeneous AII cells with Na, delayed rectifier K, and leak conductances, and an ON cone bipolar (ONCB) cell with a hyperpolarization-activated current and a leak current. All cells have a single compartment and are electrically coupled to each other. As the coupling strength decreases, mimicking the effect of MFA, the oscillation amplitude decreases, but the oscillation frequency increases in contrast to our experiments with MFA (Fig. 1*B*). All the parameters used here are the same as in Trenholm et al. (2012).

regime, while using −50 mV to put the AII in the bursting regime, capturing the rd1 AII being relatively hyperpolarized compared with the wild-type AII.

For the rest of the simulations (see Figs. 5–8, 13, and 14), an ONCB cell was electrically coupled to the three-compartmental AII cell. The ONCB cell was modeled as a passive single compartmental cell with surface area of 440 μm^2 and membrane resistivity 12,000 $\Omega \cdot cm^2$. The ONCB model was coupled to the "soma" compartment of the AII model, capturing its coupling to the AII arboreal dendrite, via a gap junction with a conductance of 750 pS. This is in the range of reported coupling strengths, which spans the range from 100 to 1,500 pS for type 5, 6, and 7 ONCB cells (Veruki and Hartveit 2002). The leak reversal potentials for the AII and the ONCB cell in this coupled AII-ONCB model were adjusted to −65 and −35 mV, respectively, to reproduce the experimentally observed membrane potentials in rd1 retinas.

RESULTS

MFA first slows down and then eliminates oscillations in rd1 retinas. It has been reported previously that the gap junction blocker MFA eliminates the oscillations in rd1 retina (Menzler and Zeck 2011; Trenholm et al. 2012). Based on this observation, it has been suggested that oscillations are an emergent property of the electrically coupled network of AII amacrine and ONCB cells. More specifically, in a model network of AIIs with slightly heterogeneous properties, electrical coupling could cause the AIIs to enter an oscillatory state even if the individual AIIs are not intrinsically oscillatory (Trenholm et al. 2012).

To characterize in more detail the effect of MFA on the AII network, we recorded membrane voltages of AII amacrine cells of rd1 mice. Our recordings confirmed spontaneous oscillatory activity in the AIIs of rd1 mice (Trenholm et al. 2012; Yee et al. 2012; Menzler and Zeck 2011; Stasheff 2008), with frequencies in the range 5–15 Hz in agreement with previous studies (Trenholm et al. 2012; Yee et al. 2012; Menzler and Zeck 2011; Stasheff 2008; Margolis et al. 2014). We then applied MFA and measured the oscillation frequency and the membrane potential of rd1 AIIs ($n = 4$). In our experiments, MFA application indeed was followed by elimination of the oscillations (Fig. 1*A*). During the onset of the MFA effect, oscillations gradually decreased in frequency as the AIIs hyperpolarized. During MFA washout, oscillation frequency increased slowly until the original frequency was restored, and the mean AII membrane potential increased at the same time. Figure 1*B* shows that oscillation frequency varied directly with membrane potential.

Next, we investigated whether such behavior during MFA application could be explained by the model put forward in Trenholm et al. (2012). In this network model, which consists of two AIIs with heterogeneous intrinsic electrical properties and one ONCB cell, it was shown that reducing the gap junction conductances is followed by elimination of the oscillations. Based on this simulation, an emergent property of a network of heterogeneous AIIs has been suggested as the source of the oscillations. In this model, the two AIIs are electrically coupled to one another and the ONCB cell is electrically coupled to one of the AIIs. The ONCB cell has a hyperpolarization-activated cationic current, a delayed rectifying K current, and a leak current. Each AII has a fast Na conductance, a delayed rectifying K conductance, and a leak conductance. Importantly, the AIIs are mildly heterogeneous in their maximal Na and leak conductances (for details, see Trenholm et al. 2012) (Fig. 2).

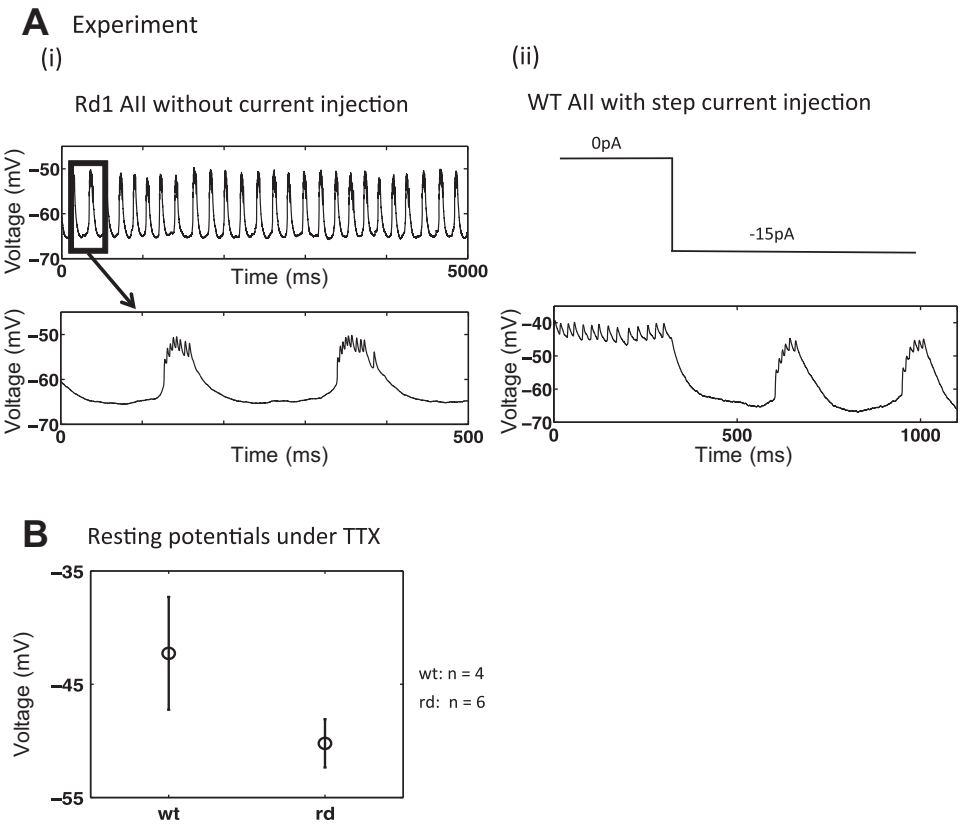

Fig. 3. Bursting in the hyperpolarized wild-type (WT) AII induces rd-like oscillations in the AII-cone bipolar network. *A*: representative intracellular rd1 and WT AII recordings. *Ai*: oscillations in rd1 AII without hyperpolarizing current injection. *Aii*: WT AII that exhibits spontaneous spikelets at rest (up to $t = 300$ ms) undergoes a transition to bursting when it is hyperpolarized (after $t = 300$ ms). *B*: under tetrodotoxin (TTX), the resting membrane potentials of WT AIIs ($n = 4$) are more depolarized than those of rd1 AIIs ($n = 6$).

We decreased the gap junction coupling strength in the model of Trenholm et al. (2012) and observed that the oscillation amplitude decreased and eventually the oscillations stopped. The oscillation frequency, however, increased during this process (Fig. 2), which is inconsistent with the experimentally observed decrease induced by MFA (Fig. 1). The marked inconsistency between the behavior of the model of Trenholm et al. (2012) and the neuronal behaviors that we observed experimentally motivated us to develop an alternative model that would describe experimentally measured parameters of rd1 oscillations.

AIIs are hyperpolarized in the rd1 retina. Upon closer inspection of the voltage waveforms recorded from rd1 AIIs, small spikelets were apparent during the depolarized phase of the oscillation (Fig. 3A*i*, *inset*) (also see Borowska et al. 2011). These oscillations were strikingly similar to those we observed previously following mild hyperpolarization of wild-type AIIs (Cembrowski et al. 2012) (Fig. 3*Aii*).

Because hyperpolarization of the membrane potential was necessary to induce bursting in wild-type AIIs, we postulated that the somatic voltages of AIIs in rd1 retinas would be hyperpolarized relative to their wild-type counterparts. Because the wild-type AIIs were spontaneously spiking (within the range of -45 to -40 mV, $n = 6$, also see Cembrowski et al. 2012) (Fig. 3*Aii*, before the hyperpolarizing current injection) and the rd1 AIIs were spontaneously oscillating (in the range of -65 to -50 mV, $n = 6$; Fig. 3*Ai*), it was not possible to compare their resting potentials directly. Therefore, we compared the resting potentials of wild-type and rd1 AIIs in the presence of TTX: although there was notable variability, the resting potentials of the rd1 AIIs under TTX were significantly more negative than those of the wild-type AIIs (-50.2 ± 2.1 mV, $n = 6$ vs. -42.3 ± 4.9 mV, $n = 4$; two-valued t-test, $P < 0.015$), as shown in Fig. 3*B*.

Rd1 oscillations resemble cable-filtered intrinsic bursting in AIIs. Previous electrophysiological and computational analyses revealed that the small somatic spikelets recorded in AIIs are attenuated versions of full action potentials initiated in an electrically distal compartment (Cembrowski et al. 2012). This referenced computational analysis made use of a multicompartmental model; single-compartment models do not describe spiking in AIIs adequately (Apollo et al. 2013).

The multicompartment model in Cembrowski et al. (2012) comprised a soma, a single spiking process, and the remainder of the dendritic tree (represented as many individual compartments) as well as experimentally constrained membrane conductances (Fig. 4*Ai*). Because the Na conductance was limited to a single, distal spike initiation site, full action potentials at this site induced only small voltage deflections ("spikelets") in the soma. Experimentally observed bursting in hyperpolarized AIIs was explained by interactions between the Na conductance and a slow, M-type K conductance that suppressed the spiking: in the bursting regime, fast spiking generated by the Na current slowly activates the M-type K current, which in turn hyperpolarizes the neuron, terminating the spiking, and completing a burst.

Because voltages in the dendrites and in the soma were predicted to be similar during bursting, we reduced the multicompartment model to a three-compartment model by lumping the soma and the dendrite into a single compartment (Fig. 4*Aii*). As in the detailed morphological model, the intrinsic bursting in the spike initiation site induced small voltage

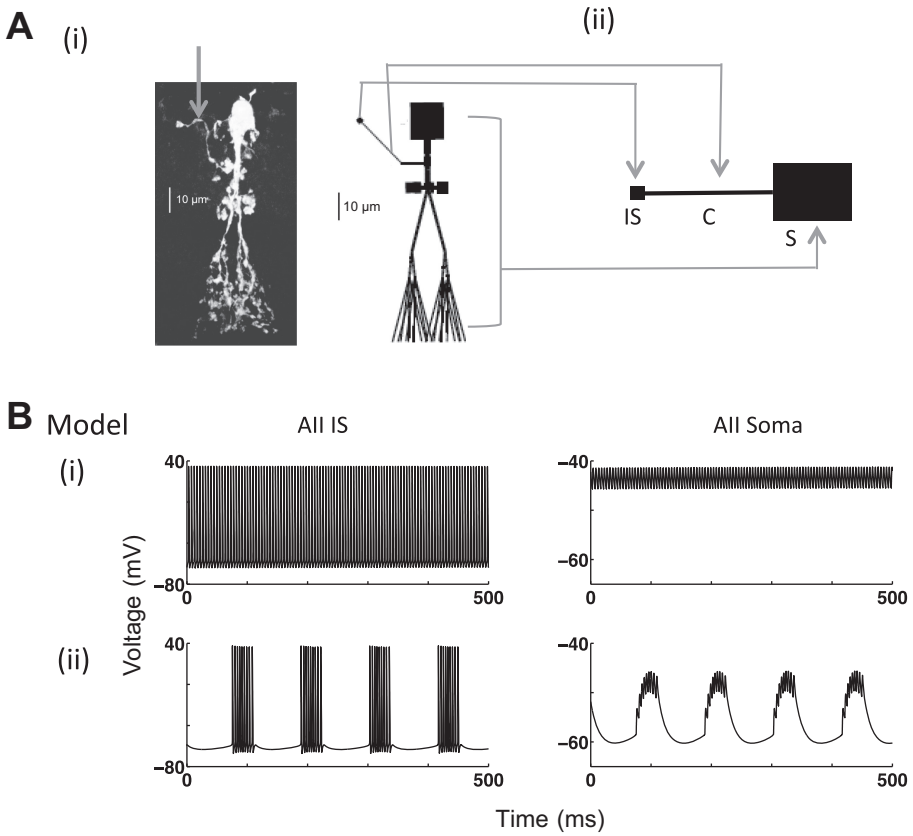

Fig. 4. Simulations showing tonic spiking and bursting of an AII. *Ai*: confocal image of an AII (*left*) and the morphologically detailed model (*right*). *Aii*: reduced 3-compartmental model of the AII consists of an "initiation site" (IS) and a "cable" (C) corresponding to the thin neurite branching from the primary dendrite of the AII (arrow in *Ai*), as well as a "soma" (S), which is taken to represent the rest of the AII (soma and dendrites). *Bi*: tonic spiking in the IS leads to small spikelets in the soma of the model wt AII. *Bii*: when the AII is hyperpolarized by lowering the leak reversal potential from -10 to -50 mV, to reproduce the experimentally observed membrane potentials of the wt and rd1 AII, the model AII shows spontaneous bursting.

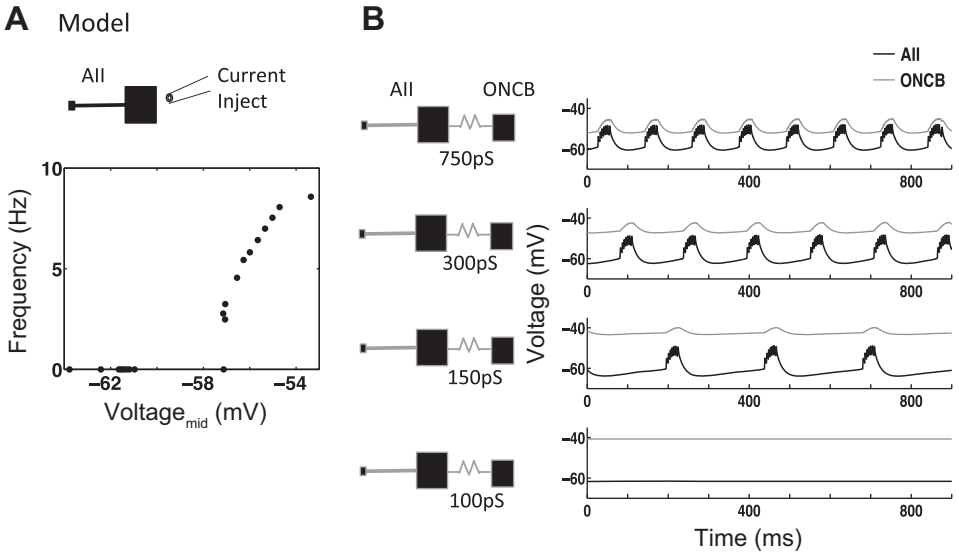

Fig. 5. Simulations support that MFA blocks oscillations via hyperpolarization of the AII. *A*: simulation of hyperpolarizing current injection to the AII. The bursting frequency is shown as a function of the midpoint of the AII membrane potential. *B*: simulation of an AII coupled to an ONCB via a gap junction. As the coupling strength of the gap junction decreases, the bursting frequency also decreases. When the coupling strength is reduced to 100 pS, bursting is eliminated.

oscillations in the soma that included small spikes during the depolarized phase (Fig. 4*Bii*).

The similarities between the voltage waveforms in the rd1 AII and the hyperpolarized wild-type AII led us to the hypothesis that oscillations in the rd1 retina reflect the intrinsic bursting activity of AIIs rather than some emergent property of an electrically coupled network. Below, we tested this hypothesis by manipulating gap junctional and K conductances in AIIs and determining whether the experimental observed effects were consistent with our model of the AII.

The model reproduces the effects of MFA on bursting in the rd1 retina. A first test of this new model is whether it correctly reproduces the slowing down and elimination of bursting due to MFA application. MFA affects the AII-ONCB network beyond blocking the coupling between AIIs; it also reduces coupling between AIIs and ONCB cells (Pan et al. 2007). Blocking electrical coupling between AIIs and ONCB cells in the rd1 retina should hyperpolarize AIIs because these ONCB cells are depolarized (V_m oscillating around −50 mV, Borowska et al. 2011) relative to AIIs (V_m oscillating around −65 to −50 mV; Fig. 3*Ai*). Our model predicts that additional hyperpolarization of bursting AIIs will suppress bursting (Fig. 5*A*). Such behavior mimics our experimental results (Fig. 1).

To test this interpretation further, we extended our model to include gap-junction coupling to a passive ONCB cell. We simulated the effect of MFA by reducing the coupling strength between the AII and the ONCB cell. As expected, weakening the coupling strength between the AII and the ONCB cell hyperpolarized the AII, which in turn decreased the oscillation frequency and then eliminated oscillations in AIIs, in agreement with our experiments (Fig. 5*B*). A similar result has been reported in Trenholm et al. (2012). If MFA stops oscillations by hyperpolarizing intrinsically oscillating AIIs, then, it should be possible to restore the oscillations by injecting depolarizing

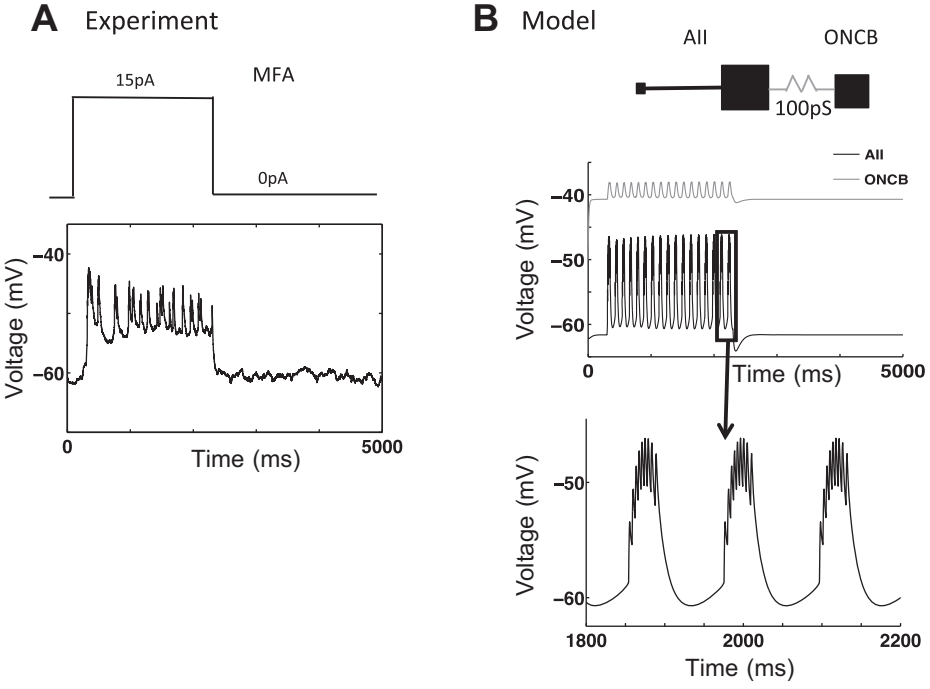

Fig. 6. Current injection following MFA application restores oscillations in rd1 AII. *A*: experimental recording from an rd1 AII in which a depolarizing current injection of 15 pA restored oscillations that had been silenced by MFA application. *B*: simulation of a depolarizing current injection of 5 pA to the model rd1 AII, with its gap junction coupling to the ONCB reduced to 100 pS to mimic the effect of MFA. The oscillations are eliminated by a reduction in the gap junction coupling (Fig. 5*B*) and are restored by the depolarizing current injection. The restored oscillations have the typical waveform (*bottom*).

current into the AII following the application of MFA. Indeed, somatic current injections of ~15–20 pA restored bursting in AIIs in both the experiments (Fig. 6*A*; $n = 4$) and the model (Fig. 6*B*).

The model accurately predicts the effects of K channel manipulation on bursting in the rd1 retina. Our model posits a central role for a M-type K conductance in bursting. Therefore, we tested the effects of potentiating and blocking M-type K conductances on bursting in AIIs of the rd1 retina to determine whether the effects were consistent with the predictions of our model. First, we tested the effect of the M-current activator flupirtine. Flupirtine is known to activate the M-type K current by shifting its activation to more negative voltages (Wu et al. 2012).

During the washin of flupirtine, oscillations first decreased in frequency and then ceased (Fig. 7, *Ai* and *Aii*). This pattern was reversed upon flupirtine washout: silenced AIIs first began to oscillate at low frequency, and then oscillation frequency rose. Concomitant with the change in frequency, the waveform of the oscillations evolved (Fig. 7*Ai*). To quantify the change in the waveform, we measured the width of the bursts at a membrane potential that corresponded to 30% of the maximal oscillation amplitude in each sweep (1,667-ms long). As Fig. 7, *Aiii* and *Aiv*, shows, the bursts became narrower during the washin of flupirtine (from 79.3 ± 4.5 to 44.9 ± 9.5 ms). The effect due to flupirtine was found to be significant ($P < 10^{-3}$ by two-way ANOVA). Biophysically, with the left shift of the activation curve of the M current fewer spikes are required to generate an outward current sufficient to shut off the spiking.

We also simulated the effect of flupirtine in our model AII by shifting the half-activation voltage ($V_{1/2}$) of the M-type K current to more negative voltages. Consistent with the experiments, this manipulation decreased bursting frequency and then silenced the cell (Fig. 7*B*). While the frequency generally decreased as $V_{1/2}$ of the M current became more negative, there were also discrete jumps around $V_{1/2} = -42$ mV and $V_{1/2} =$

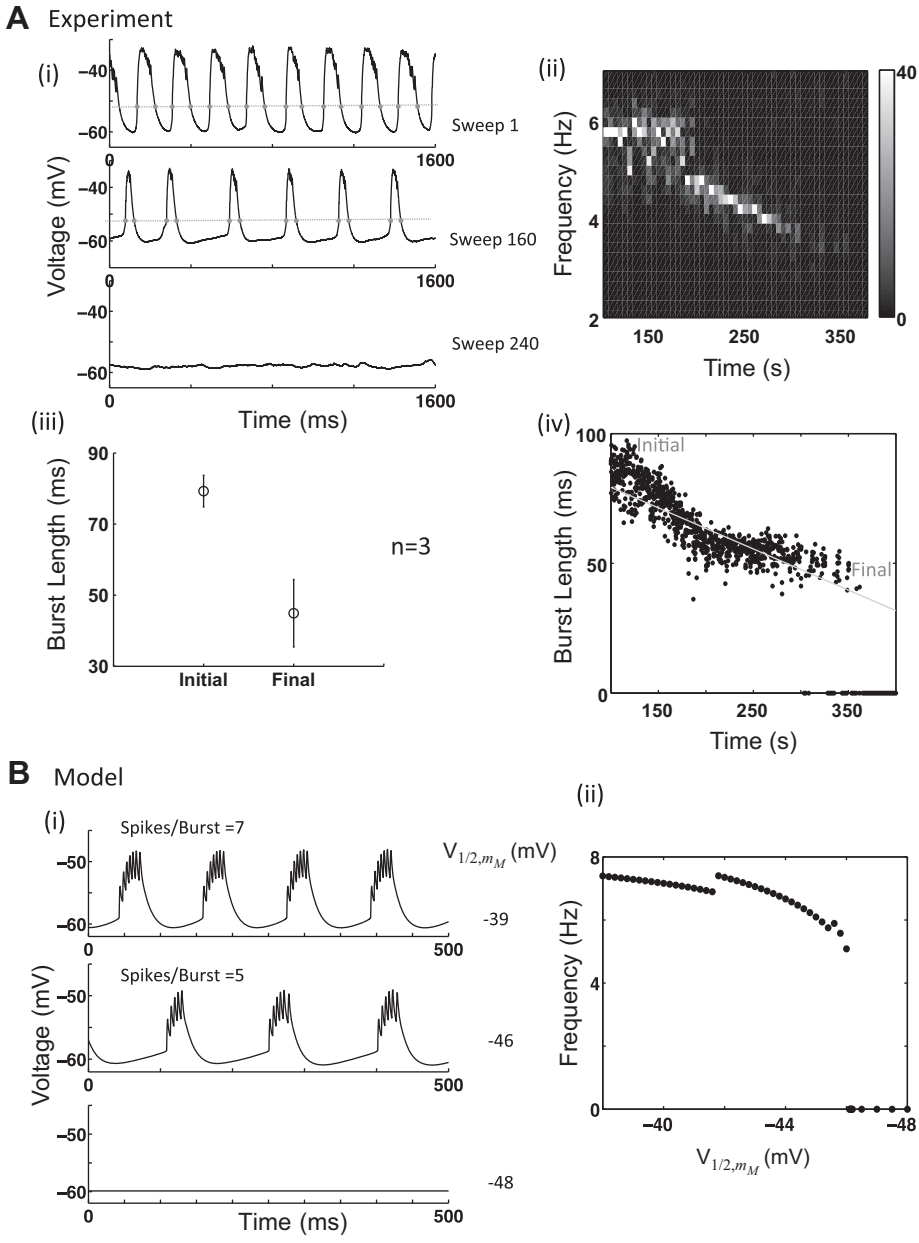

Fig. 7. Opening M current reduces frequency and burst length and stops oscillations. *A*: experiment during flupirtine washin on an rd1 AII. *Ai*: representative traces of the AII membrane potential during flupirtine washin. *Aii*: spectrogram of the recording in *Ai* shows that the frequency decreased under flupirtine application, eventually resulting in termination of the oscillations. *Aiii*: burst length at the end of the flupirtine washin (final) is significantly smaller than at the beginning (initial) ($n = 3$; $P < 10^{-3}$). *Aiv*: burst length during the flupirtine washin of a representative recording. The length was measured at 30% of the maximal oscillation amplitude for each 1,667-ms-long sweep (dotted line in *Ai*). "Initial" and "Final" indicate where the initial and final burst lengths were measured. *B*: simulation mimicking flupirtine application by moving the half-activation voltage $V_{1/2}$ of the M conductance leftward. *Bi*: representative membrane potential traces for the model AII. Along with the frequency decrease, the number of spikes per burst decreases as well, resulting in a burst length decrease. *Bii*: in the model the burst frequency decreases as the half-activation voltage $V_{1/2}$ of the M conductance is reduced. The discrete jumps correspond to reduction in the number of spikes per burst. Eventually the AII becomes quiescent.

−45 mV (Fig. 7*Bii*). These jumps occurred due to a reduction in the number of spikes per burst. In the experiments the individual bursts were too variable to allow the identification of such details (cf. Fig. 3*Ai*). As in the experiment, however, the burst width decreased (Fig. 7*Bi*).

To determine how antagonizing the M-type K channel affects the rd1 oscillations, we used LP (see Cembrowski et al. 2012). Blocking the M current reduced the burst frequency (Fig. 8, *Ai* and *Aii*; $n = 5$). The burst duration, however, increased from 87.4 ± 41.1 to 175.0 ± 34.7 ms; this is opposite to the effect of flupirtine on the burst duration. Despite its marked variation across the recorded cells, the increase was highly significant ($P < 10^{-3}$; Fig. 8, *Aiii* and *Aiv*). In agreement with this observation, the computational model also generated lower burst frequencies and longer burst durations when the maximal M conductance was reduced (Fig. 8*B*). This was expected, since the M current has been identified as being responsible for terminating spiking (Cembrowski et al. 2012).

In the model, decreasing the M current caused the burst duration to increase without bound and eventually change to tonic spiking. In the experiments, however, LP did not eliminate all oscillations and it did not induce tonic spiking. Instead, when the burst duration increased beyond ~200 ms, a transition to a different type of low-frequency (~1 Hz) oscillation occurred (Figs. 8*Ai*, *bottom*, and 9*B*). Riding on top of these slow oscillations were faster, irregular, 5- to 10-Hz bursts of spikes. These bursts were reminiscent of the characteristic rd1 oscillations that we observed in the absence of LP. This phenomenon was also observed when ONCB cells first were hyperpolarized by application of L-AP4, which on its own does not block oscillations in the rd1 retina (Borowska et al. 2011) ($n = 6$). Because of this transition to a qualitatively different type of oscillation, the measurement of the increase in the burst duration due to LP depended on the identification of the

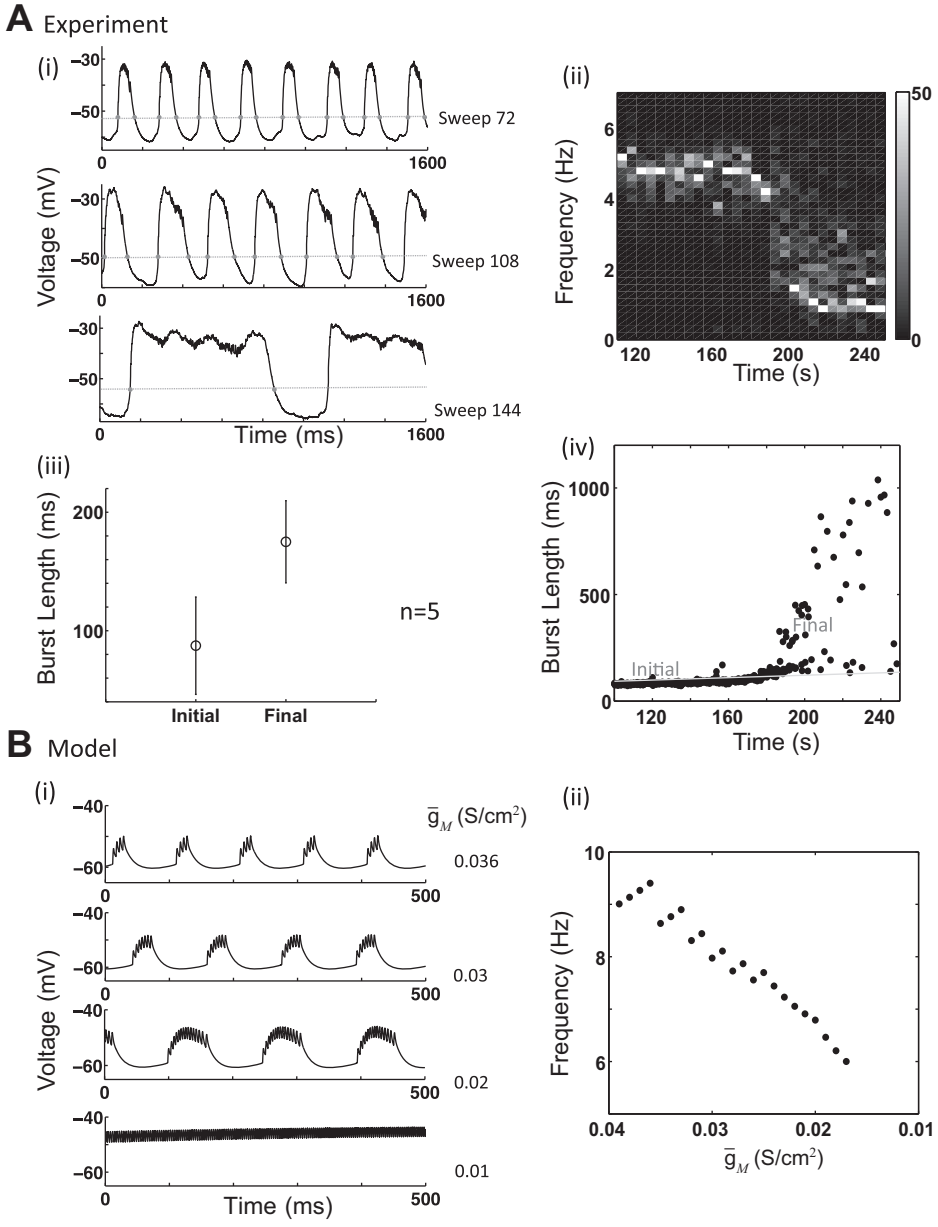

Fig. 8. Blocking M current reduces frequency and increases burst length. *A*: experiment during linopiridine hydrochloride (LP) washin on an rd1 AII. *Ai*: representative traces of the AII membrane potential during LP washin. The trace corresponding to the ~1-Hz frequency (*bottom*) had a characteristic waveform consisting of overshoots and a plateau that differed from the waveform of the typical rd1 oscillations. *Aii*: spectrogram of the recording in *Ai* shows that the frequency decreased under LP application, eventually reaching a very low frequency of ~1 Hz. *Aiii*: initial and the final burst lengths during LP washin show a significant increase ($n = 5$, $P < 10^{-3}$). The final burst lengths were measured right before the transition to the ~1-Hz oscillations. *Aiv*: burst length increase during the LP washin of a representative recording. The length was measured at 30% of the maximal oscillation amplitude for each 1,667-ms-long sweep (dotted line in *Ai*). "Initial" and "Final" indicate where the initial and final burst lengths were measured. *B*: simulation mimicking LP application by reducing the M-current maximal conductance $\bar{g}_M$. *Bi*: representative membrane potential traces for the model AII. While the burst frequency decreases, the number of spikes per burst increases, resulting in a burst length increase. *Bii*: in the model the burst frequency decreases as the M-conductance decreases. The discrete jumps correspond to an increase in the number of spikes per burst. Below $g_M = 0.015$ S/cm^2, the AII exhibits tonic spiking.

transition time. We used the sudden increase in the variability of the duration as a criterion for that transition.

The slow-frequency oscillation resembled both in frequency and shape the slow, Ca channel-mediated oscillations that have been observed in ONCB cells of rat, mouse, and goldfish retina when inhibition was blocked (Ma and Pan 2003; Yee et al. 2012; Zenisek and Matthews 1998). To test whether the slow oscillations were indeed Ca channel mediated, we applied cadmium (Cd^{2+}) and nickel (Ni^{2+}), two nonselective voltage-gated Ca^{2+} channel blockers, after the slow oscillations induced by LP had been established (in the presence of L-AP4; $n = 4$). The characteristic shape and frequency of the slow oscillations induced by LP were disrupted by Ni^{2+} and Cd^{2+}, supporting our hypothesis that the slow oscillations that appear under LP application require Ca channels and therefore arise from a mechanism that differs from that underlying the ~10-Hz oscillations (Fig. 9).

Thus either blocking or potentiating an M-type K conductance eliminates the characteristic 5- to 10-Hz oscillations in rd1 AIIs (Figs. 7 and 8). The observed changes in oscillation frequency and burst duration are predicted by our model of a single AII. This suggests that the slow M-type K current plays the same key role in generating the rd1 oscillations as it does in generating bursting in wild-type AIIs.

Note that the model investigated in Trenholm et al. (2012) does not include an M current and does therefore not allow any predictions pertaining to these experiments.

Intrinsic oscillations in AIIs are propagated unaltered to ganglion cells of the rd1 retina. In rd1 retina, the 5- to 15-Hz oscillations are also observed in retinal ganglion cells (RGCs). These oscillations reflect rhythmic synaptic input (Margolis et al. 2008; Borowska et al. 2011; Menzler and Zeck 2011; Stasheff 2008; Ye and Goo 2007; Yee et al. 2012), and anticorrelation of activity in ON and OFF alpha RGCs implicates the AII as a major contributor to this synaptic input (Margolis et al. 2014). Here, having found evidence to support the hypothesis that the rd1 oscillations in AIIs are intrinsically generated by their M-type K conductances, next we investigated whether these AII oscillations are indeed the origin of the RGC oscillations by testing the effects of LP and flupirtine on the oscillations in RGCs in the rd1 retina. The oscillations were measured with intracellular recordings of single alpha ganglion cells in the rd1 whole mount retina and by extracellular recordings of single and multiunits via MEA.

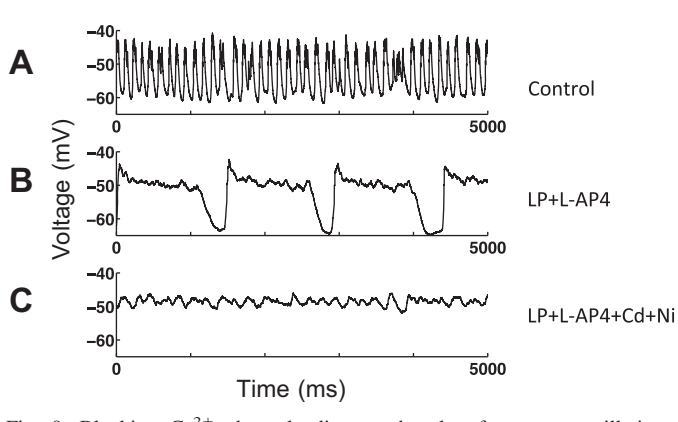

Fig. 9. Blocking Ca^{2+} channels disrupts the slow-frequency oscillations. *A*: representative recording of an rd1 AII under LP and Ca^{2+} blockers. The characteristic rd1 oscillations, which were unaffected by L-(+)-2-amino-4-phosphonobutyric acid (L-AP4; *A*), were disrupted by LP and replaced by slow-frequency oscillations (*B*). The slow-frequency oscillations were eliminated by Ni^{2+} and Cd^{2+} (*C*).

Both flupirtine and LP disrupted oscillatory synaptic currents and membrane potentials recorded in the whole cell configuration in ON and OFF alpha RGCs. Observed changes in frequency and burst duration were consistent with those of AII oscillations; flupirtine eliminated the oscillations following a decrease in both frequency and burst duration, and LP decreased the bursting frequency and increased the burst duration before eliminating the rd1 oscillations. Representative traces of ganglion cell membrane potentials along with their frequency and burst duration changes under flupirtine and LP are shown in Figs. 10, *Ai*, *Aii*, and *Aiv*, and *Bi*, *Bii*, and *Biv*, respectively. Figure 10, *Aiii* and *Biii*, shows the collective data of burst duration changes under flupirtine and LP. In retinas treated with LP ($n = 4$), the width of ganglion cell bursting increased (from 38.5 ± 27.8 to 305.3 ± 108.5 ms, $P < 10^{-3}$). In three out of four cells under flupirtine, the burst widths decreased (from 51.7 ± 12.4 to 17.4 ± 8.4 ms, $P < 10^{-3}$). In one case, application of flupirtine was followed by almost instant elimination of the oscillations, so it was not possible to observe slow changes in the burst duration. In addition, in three out of four cells treated with flupirtine, the bursting frequency became irregular before the cells became quiescent. However, in all cases, the spikes became less frequent after flupirtine application.

In the extracellular electrode recordings, we studied the oscillations present in each single unit as well as in the multiunit activity (MUA). Both single and multiunit activities agreed with the changes in AII oscillations under LP application. A representative single unit activity is shown in Fig. 11*A*. It is apparent that the oscillations under LP are slower than those in L-AP4 and washout conditions. Similarly, the interspike intervals show a nonzero peak at a much higher value (810 ms) under LP than under L-AP4 or washout. Figure 11*B* shows the comprehensive bursting statistics of single units. Under L-AP4 ($n = 61$), the single unit burst lengths had a median value of 49 ms with an interquartile range (IQR) of 45–59 ms. The frequency of these oscillations had a median 6.2 Hz with IQR 4.8–6.7 Hz. When LP was applied, the burst lengths of the single units ($n = 18$) increased to 64 ms and their IQR ranged from 40 to 120 ms. The frequency of these oscillations decreased to a median of 1.37 Hz with an IQR of 1.08–1.6 Hz, consistent with what we observed from AIIs under LP. Then, for the washout condition, the oscillation frequencies of the single units ($n = 34$) increased back to near the values found for the initial L-AP4 condition, and the mean burst length decreased to 51 ms, with IQR = 39–67 ms.

We also inspected the effects of LP on MUA. The spectograms of the MUA in Fig. 12*A* show that LP application slowed down the MUA oscillations. Based on the MUA, oscillating channels under the L-AP4 condition ($n = 52$) had a median oscillation frequency of 7.5 Hz and an IQR of 4.8–9.6 Hz. For the LP condition ($n = 70$), the oscillating channels had a median frequency of 1.75 Hz and IQR of 1.2–4.8 Hz. Then, for the washout condition ($n = 66$), we observed that the oscillation frequencies increased back towards their initial values (Fig. 12*B*).

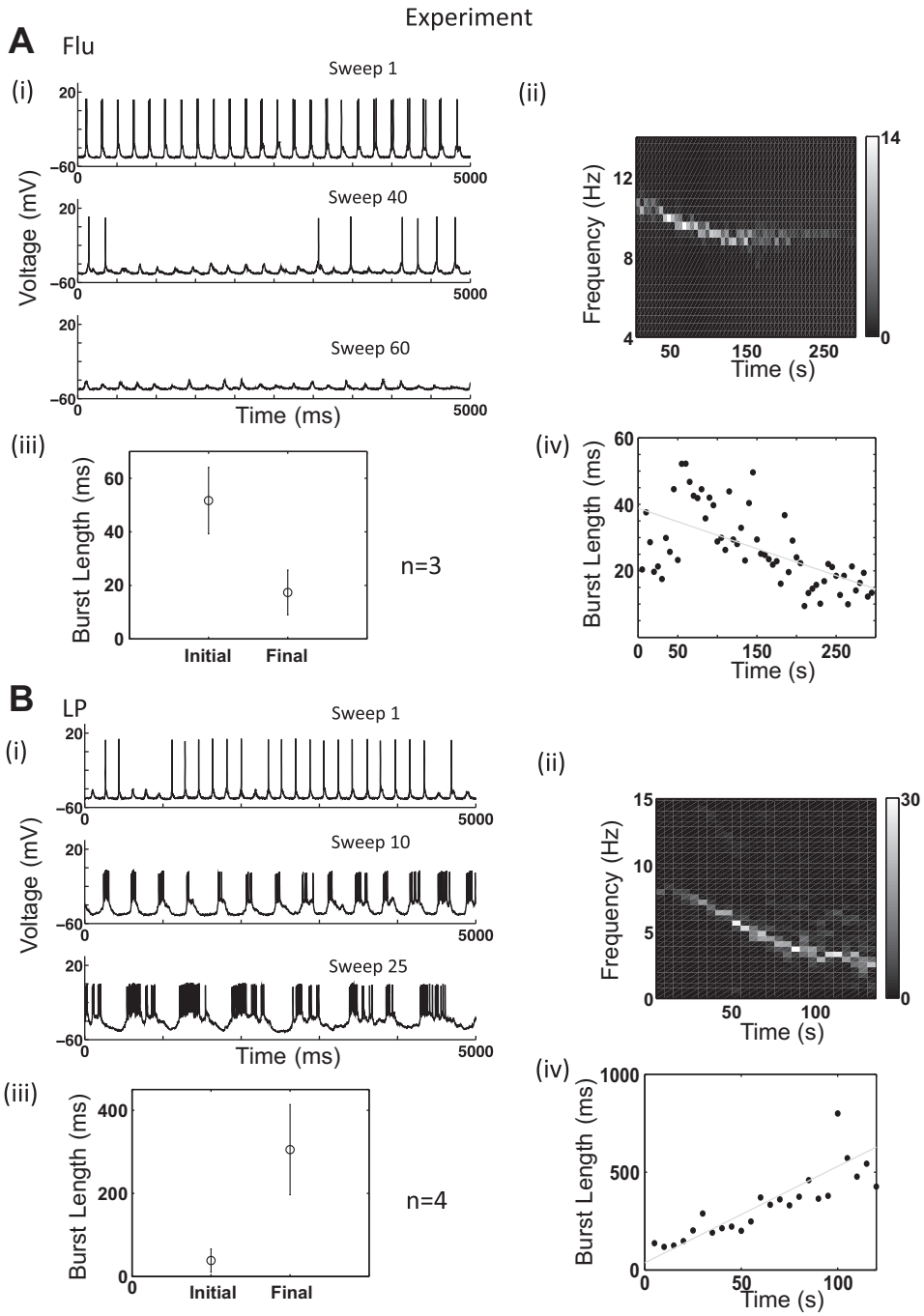

Fig. 10. The intracellularly recorded rd1 oscillations in retinal ganglion cells (RGCs) change similarly to those in AIIs under M-current activator and blocker. *A*: rd1 oscillations in RGCs were disrupted in the presence of flupirtine. *Ai*: representative RGC membrane potential under flupirtine. Flupirtine decreased oscillation frequency (*Aii*) and decreased burst duration (*Aiv*). *Aiii*: initial and the final burst lengths during flupirtine washin show a significant decrease ($n = 3$, $P < 10^{-3}$). *B*: rd1 oscillations in RGCs were disrupted in the presence of LP. *Bi*: representative RGC membrane potential under LP. LP induced a decrease in oscillation frequency (*Bii*) and increase in burst duration (*Biv*). The burst durations were averaged for each 5-s-long sweep. *Biii*: initial and the final burst lengths during LP washin show a significant increase ($n = 4$; $P < 10^{-3}$).

The extracellular recordings were also made under flupirtine (2 experiments), and we observed either complete elimination of the oscillations or a decreased bursting frequency. However, we do not report extracellular recording summary statistics here for the bursting activity of RGCs under flupirtine, because we did not isolate a statistically significant number of single units for this condition ($n = 7$).

In conclusion, intracellular recordings, single unit extracellular recordings, and multiunit extracellular recordings all show elimination of the oscillatory activities in RGCs under LP and flupirtine. Moreover, the changes in burst frequency and burst duration in RGCs agree with those in AIIs, providing strong evidence that the oscillations in RGCs indeed come from the upstream AII cells in the rd1 retina.

DISCUSSION

A combined experimental and computational approach was used to test the hypothesis that oscillations of AIIs in the rd1 retina are intrinsic and the result of interactions between fast, depolarizing Na and slow, hyperpolarizing, M-type K conductances. In this scenario, the oscillations arise as the result of spontaneous bursting in a distal compartment, generated because rd1 AIIs are hyperpolarized relative to wild-type AIIs. We analyzed a compartmental model of the AII (Cembrowski et al. 2012) to predict the expected electrophysiological responses of AIIs to pharmacological manipulation of M-type K currents and performed these experiments. The combined computational and exper-

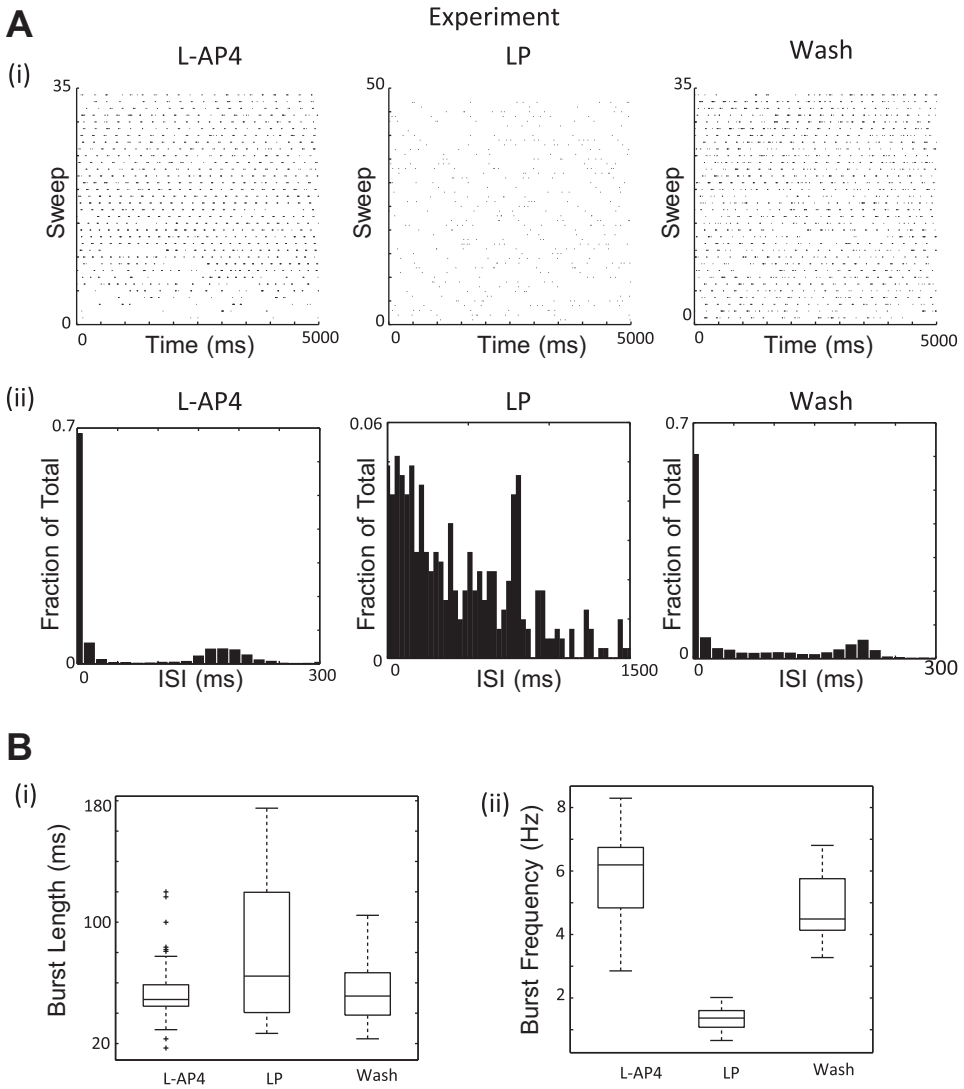

Fig. 11. The extracellular recordings of single RGCs show elimination of the oscillations under M-current blocker. *A*: representative single unit. *Ai*: raster plots under L-AP4, LP, and washout conditions of a representative single unit and their (*Aii*) interspike interval (ISI) distributions with 15- and 30-ms bin sizes for L-AP4/washout and LP conditions, respectively. Under LP condition, the nonzero peak of the ISI distribution occurs ~810 ms, which is significantly higher than under L-AP4 (180 ms) and washout (210 ms). The raster plot under LP also shows slower rhythmic activity compared with L-AP4 and washout conditions. *B*: single unit bursting statistics. *Bi*: mean burst length for L-AP4, LP, and washout conditions. *Bii*: oscillation frequency for L-AP4, LP, and washout conditions.

imental results are fully consistent with our hypothesis. Additionally, single cell and multielectrode array recordings from ganglion cells demonstrated that altered AII activity was propagated unchanged to ganglion cells. Our conclusion is that the oscillatory output of ganglion cells in the rd1 retina reflects the intrinsic properties of AII amacrine cells.

Mechanisms underlying bursting in neurons in the rd1 retina. Spontaneous oscillatory activity in interneurons of the rd1 retina has been documented in a number of studies (Borowska et al. 2011; Margolis et al. 2014; Toychiev et al. 2013; Trenholm et al. 2012). Because blocking electrical transmission among AIIs and between AIIs and ONCB cells inhibits

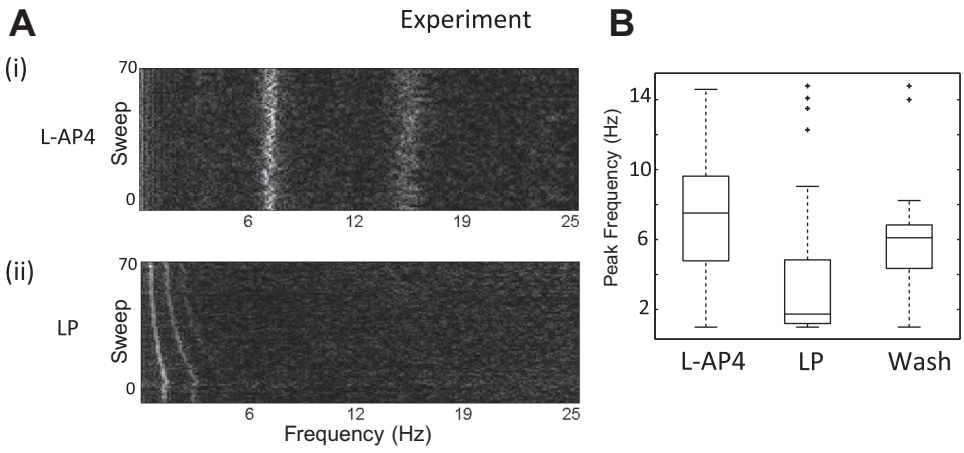

Fig. 12. The multiunit activity (MUA) of the extracellular recordings shows dependency of the RGC oscillations on M current. MUA oscillation analysis. *A*: example channel MUA oscillations under L-AP4 and LP conditions. The spectrograms are in 5-s-long sweeps with a 2.5-s overlap. For the MUA, 52 channels had oscillatory activity for the L-AP4 condition, 70 channels had oscillatory activity for the LP condition, and 66 channels had oscillatory activity for the washout condition. *B*: boxplot of MUA oscillation frequencies under L-AP4, LP, and washout conditions.

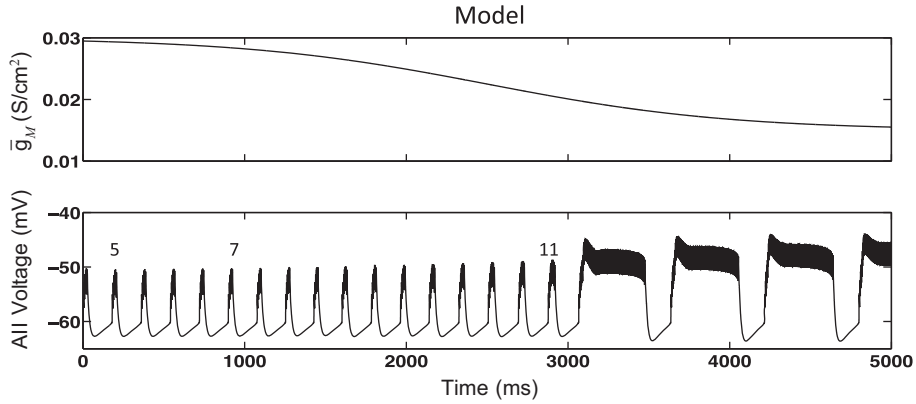

Fig. 13. FitzHugh-Nagumo type model of Ca^{2+}-mediated slow oscillations in an ONCB coupled to an AII. In this simulation, $\bar{g}_M$ decreases in a sigmoidal fashion mimicking LP application. The burst duration increases, and when it reaches a critical value, the waveform makes a transition from the characteristic rd1 oscillations to qualitatively different slow oscillations. The number of spikes per burst with decreasing $\bar{g}_M$ increases as indicated.

it, this activity has been characterized as an emergent property of a network of heterogeneous neurons (Trenholm et al. 2012).

Our study, however, supports a different conclusion: oscillations in the rd1 retina are explained largely by the intrinsic properties of AII amacrine cells, which appear to rest at potentials hyperpolarized relative to those observed in wild-type AIIs (Fig. 3). A number of experimental results, predicted by our compartmental model of the AII, support this assertion. In particular, the burst waveforms of AIIs in the rd1 retina closely resemble bursts in wild-type AIIs elicited by hyperpolarization (Fig. 3). Our compartmental model reproduces these bursts, and this allowed us to make predictions about the characteristics of bursting, specifically about the role played by M-type K currents, that then could be tested experimentally.

Our model suggested that potentiating the M current would first reduce burst duration and decrease oscillation frequency and then eliminate the oscillations and that blocking the M current would increase burst duration and decrease oscillation frequency; these predictions were borne out by our experiments (Figs. 7 and 8). The corresponding effects of pharmacological manipulation of M currents were also observed in ganglion cells (Figs. 10–12), indicating that activity in AIIs is propagated unchanged to ganglion cells.

Bursting by AIIs is generated intrinsically in our model, which suggests that hyperpolarization of AIIs in rd1 mice may be the primary cause of oscillations. Because our model was developed in a study of wild-type AIIs (Cembrowski et al. 2012), we suggest that AIIs in rd1 retinas are functionally similar to their wild-type counterparts. Consistent with this notion, TTX blocks bursting in rd1 AIIs, as it does in wild-type AIIs (Cembrowski et al. 2012; Trenholm et al. 2012; Margolis et al. 2014). The lower concentration of TTX used in Menzler and Zeck (2011), however, did not eliminate the oscillations in the local field potential associated with oscillations in ganglion cells of the rd1 mouse.

Taken together, the rd1 oscillations are cable-filtered bursts generated by the interplay between the fast, spike-generating Na and the slowly activating M-type K conductances. When the AIIs are relatively depolarized as in the wild-type retinas, the cells exhibit spontaneous tonic spiking, while too much hyperpolarization brings the cells to the quiescent regime. However, in between, there is a range of

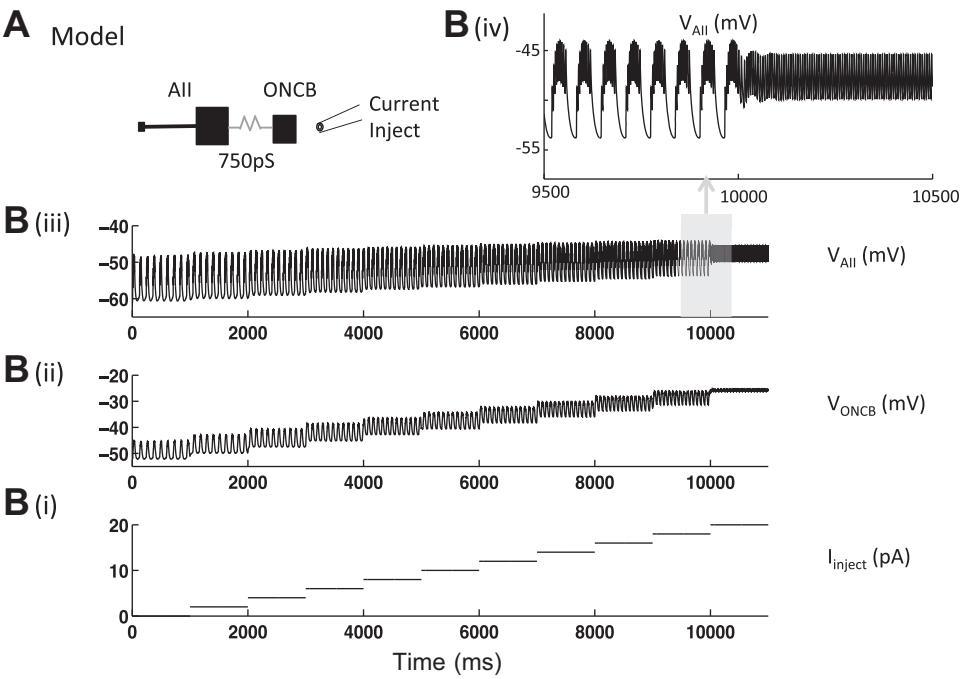

Fig. 14. In the model, depolarizing current injection into an ONCB suppresses bursting in the coupled AII. *A*: passive ONCB is coupled to an AII cell with a coupling strength of 750 pS. *B*: current injection of 20 pA in the ONCB (*Bi*) depolarizes the ONCB (*Bii*) and eliminates bursting in the coupled AII (*Biii* and *Biv*).

membrane potential that induces spontaneous bursting in the AIIs.

As others have observed (Trenholm et al. 2012), in our experiments an antagonist of gap junctions slowed and then blocked oscillations in the rd1 retina (Fig. 1); our model predicts this as well (Fig. 5). Moreover, our model further predicted, and our experiments confirmed, that bursting in individual AIIs in the presence of MFA can be restored by injection of depolarizing current (Fig. 6). This supports that the oscillations arise from individual AIIs, not from a network effect as previously suggested (Trenholm et al. 2012). Based on these results, we suggest that the main effect of MFA is hyperpolarization of AIIs through elimination of their coupling to more depolarized ONCB cells. Thus our study supports the conclusion that homotypic electrical coupling between AIIs does not contribute to bursting by AIIs and that heterotypic electrical coupling between AIIs and ONCB cells is relevant primarily because it affects the membrane potentials of AIIs.

Slow Ca channel-dependent oscillations. We found that application of the M-current antagonist LP reduced oscillation frequency and lengthened the burst duration, consistent with our model (Fig. 8). LP, however, also induced slow (~1 Hz) oscillations in AIIs that appeared to involve Ca channels (Fig. 9). The frequency and waveforms of bursts underlying these slow oscillations resembled Ca channel-dependent regenerative activity observed previously in isolated ONCB cells (Ma and Pan 2003) and in whole retinas when inhibition was blocked (Yee et al. 2012). We speculate that the enhanced burst duration in the presence of LP may allow activity in AIIs to trigger such regenerative events in ONCB cells; in turn, the regenerative events in ONCB cells modulate the AII voltage.

To illustrate the feasibility of such a scenario, we extended our passive ONCB cell model to include a simple model of FitzHugh-Nagumo type (Fitzhugh 1961) to allow for regenerative events; active ONCB cells were coupled to model AIIs (Choi 2014). In this simulation, decreasing the maximal M-type K conductance to mimic LP application generated a sudden transition from short bursts to much longer depolarizing events upon which spiking was superimposed (Fig. 13). We did not, however, assess whether this model captured all aspects of the experimentally observed transition to the slow oscillations induced by LP; while this is an interesting question, we considered it to be beyond the scope of the current work.

Clinical implications. A recent study demonstrates that MFA blocks the characteristic oscillatory activity of retinas of rd10 mice, which have a less severe retinal degeneration phenotype than rd1 mice, and improves signal transmission from surviving photoreceptors to ganglion cells (Toychiev et al. 2013). This finding is difficult to interpret, however, since gap junctions mediate interactions among many different classes of retinal neurons. Thus blocking all gap junctions may not be the most advantageous therapeutic intervention.

Our study indicates that MFA application eliminates oscillations not by uncoupling the AII network but by hyperpolarizing intrinsically active AIIs. As a result, manipulating the resting membrane potential of AIIs in some other manner might be an effective and benign way to restore signaling in a deteriorating retina. Introducing light sensitivity into bipolar cells (Lagali et al. 2008; Doroudchi et al. 2011) or stimulating them with retinal prostheses (Stingl et al. 2013) are possibilities that may be sufficient to reduce hyperpolarization of AIIs and keep them from bursting.

In recent optogenetic experiments, introducing channel rhodopsin-2 expression in ON bipolar cells via electroporation (Lagali et al. 2008) or viral vectors (Doroudchi et al. 2011) has been successful in restoring light-induced responses both physiologically and behaviorally. Therefore, it will be interesting to examine how effective such light sensitivity is in suppressing the rd1 oscillations. To predict how much depolarization in ONCB cells is needed to suppress the oscillations, depolarization of the ONCB cell was simulated via current injections in our model of a passive ONCB cell electrically coupled to an AII cell with the coupling strength of 750 pS (Fig. 14). In our model, a current injection of 20 pA, which resulted in an ~20-mV depolarization in the coupled ONCB, suppressed the oscillatory activities in the AII and induced tonic spiking. Although variability in coupling strengths and number of coupled ONCB cells prevents us from predicting the precise amount of depolarization needed, this simulation predicts that depolarization of ~20 mV in ONCB cells is sufficient to eliminate the oscillations in the coupled AIIs. Whether current methods of introducing light sensitivity in ON bipolar cells can bring the rd1 retina to the nonbursting regime would be an interesting topic for future work.

ACKNOWLEDGMENTS

We thank Rosemary Braun for many helpful discussions and Jiji Jiang for technical support.

GRANTS

This study was supported by National Eye Institute Grants EY-017836 (to J. H. Singer) and EY-021372 (to W. L. Kath, H. Riecke, and J. H. Singer). J. H. Singer was a Research to Prevent Blindness Special Scholar for Retinitis Pigmentosa.

DISCLOSURES

No conflicts of interest, financial or otherwise, are declared by the author(s).

AUTHOR CONTRIBUTIONS

Author contributions: H.C., L.Z., M.S.C., W.L.K., J.H.S., and H.R. conception and design of research; H.C., L.Z., C.F.S., D.A.B., J.H.S., and H.R. analyzed data; H.C., M.S.C., C.F.S., A.L.M., D.A.B., W.L.K., J.H.S., and H.R. interpreted results of experiments; H.C. prepared figures; H.C. and H.R. drafted manuscript; H.C., M.S.C., C.F.S., W.L.K., J.H.S., and H.R. edited and revised manuscript; H.C., W.L.K., J.H.S., and H.R. approved final version of manuscript; L.Z. and A.L.M. performed experiments.

REFERENCES

Adams NA, Awadein A, Toma HS. The retinal ciliopathies. *Ophthalmic Genet* 28: 113–125, 2007.

Apollo N, Grayden DB, Burkitt AN, Meffin H, Kameneva T. Modeling intrinsic electrophysiology of AII amacrine cells: preliminary results. *Conf Proc IEEE Eng Med Biol Soc* 2013: 6551–6554, 2013.

Borowska J, Trenholm S, Awatramani GB. An intrinsic neural oscillator in the degenerating mouse retina. *J Neurosci* 31: 5000–5012, 2011.

Carter-Dawson LD, LaVail MM, Sidman RL. Differential effect of the rd mutation on rods and cones in the mouse retina. *Invest Ophthalmol Vis Sci* 17: 489–498, 1978.

Cembrowski MS, Logan SM, Tian M, Jia L, Li W, Kath WL, Riecke H, Singer JH. The mechanisms of repetitive spike generation in an axonless retinal interneuron. *Cell Rep* 1: 155–166, 2012.

Chang B, Hawes NL, Hurd RE, Davisson MT, Nusinowitz S, Heckenlively JR. Retinal degeneration mutants in the mouse. *Vision Res* 42: 517–525, 2002.

Chang B, Hawes NL, Pardue MT, German AM, Hurd RE, Davisson MT, Nusinowitz S, Rengarajan K, Boyd AP, Sidney SS, Phillips MJ, Stewart RE, Chaudhury R, Nickerson JM, Heckenlively JR, Boatright JH. Two mouse retinal degenerations caused by missense mutations in the beta-subunit of rod cGMP phosphodiesterase gene. *Vision Res* 47: 624–633, 2007.

Choi H. *Modeling of Oscillations and Bursting in Retinal AII Amacrine Cells* (PhD thesis). Evanston, IL: Northwestern Univ., 2014.

Demb JB, Singer JH. Intrinsic properties, and functional circuitry of the AII amacrine cell. *Vis Neurosci* 29: 51–60, 2012.

Doroudchi MM, Greenberg KP, Liu J, Silka KA, Boyden ES, Lockridge JA, Arman AC, Janani R, Boye SE, Boye SL, Gordon GM, Matteo BC, Sampath AP, Hauswirth WW, Horsager A. Virally delivered channelrhodopsin-2 safely and effectively restores visual function in multiple mouse models of blindness. *Mol Ther* 19: 1220–1229, 2011.

Fine I, Wade A, Brewer A, May M, Goodman D, Boynton G, Wandell B, MacLeod D. Long-term deprivation affects visual perception and cortex. *Nat Neurosci* 6: 915–916, 2003.

Fitzhugh R. Impulses and physiological states in theoretical models of nerve membrane. *Biophys J* 1: 445–466, 1961.

Habermann C, O'Brien B, Wassle H, Protti D. AII amacrine cells express L-type calcium channels at their output synapses. *J Neurosci* 23: 6904–6913, 2003.

Harris KD, Hirase H, Leinekugel X, Henze DA, Buzsaki G. Temporal interaction between single spikes and complex spike bursts in hippocampal pyramidal cells. *Neuron* 32: 141–149, 2001.

Hartong DT, Berson EL, Dryja TP. Retinitis pigmentosa. *Lancet* 368: 1795–1809, 2006.

Jimenez AJ, Garcia-Fernandez JM, Gonzalez B, Foster RG. The spatio-temporal pattern of photoreceptor degeneration in the aged rd/rd mouse retina. *Cell Tissue Res* 284: 193–202, 1996.

Lagali P, Balya D, Awatramani G, Munch T, Kim D, Busskamp V, Cepko C, Roska B. Light-activated channels targeted to ON bipolar cells restore visual function in retinal degeneration. *Nat Neurosci* 11: 667–675, 2008.

Ma YP, Pan ZH. Spontaneous regenerative activity in mammalian retinal bipolar cells: roles of multiple subtypes of voltage-dependent Ca^{2+} channels. *Vis Neurosci* 20: 131–139, 2003.

Marc RE, Jones BW, Anderson JR, Kinard K, Marshak DW, Wilson JH, Wensel T, Lucas RJ. Neural reprogramming in retinal degeneration. *Invest Ophthalmol Vis Sci* 48: 3364–3371, 2007.

Margolis DJ, Gartland AJ, Singer JH, Detwiler PB. Network oscillations drive correlated spiking of ON and OFF ganglion cells in the rd1 mouse model of retinal degeneration. *PLoS One* 9: e86253, 2014.

Margolis DJ, Newkirk G, Euler T, Detwiler PB. Functional stability of retinal ganglion cells after degeneration-induced changes in synaptic input. *J Neurosci* 28: 6526–6536, 2008.

Menzler J, Zeck G. Network oscillations in rod-degenerated mouse retinas. *J Neurosci* 31: 2280–2291, 2011.

Murphy G, Rieke F. Network variability limits stimulus-evoked spike timing precision in retinal ganglion cells. *Neuron* 52: 511–524, 2006.

Pan F, Mills SL, Massey SC. Screening of gap junction antagonists on dye coupling in the rabbit retina. *Vis Neurosci* 24: 609–618, 2007.

Quiroga RQ, Nadasdy Z, Ben-Shaul Y. Unsupervised spike detection and sorting with wavelets and superparamagnetic clustering. *Neural Comput* 16: 1661–1687, 2004.

Schmitzer-Torbert N, Jackson J, Henze D, Harris K, Redish AD. Quantitative measures of cluster quality for use in extracellular recordings. *Neuroscience* 131: 1–11, 2005.

Schmitzer-Torbert N, Redish AD. Neuronal activity in the rodent dorsal striatum in sequential navigation: separation of spatial, and reward responses on the multiple T task. *J Neurophysiol* 91: 2259–2272, 2004.

Stasheff SF. Emergence of sustained spontaneous hyperactivity, and temporary preservation of OFF responses in ganglion cells of the retinal degeneration (rd1) mouse. *J Neurophysiol* 99: 1408–1421, 2008.

Stingl K, Bartz-Schmidt K, Besch D, Braun A, Bruckmann A, Gekeler F, Greppmaier U, Hipp S, Hortdorfer G, Kernstock C, Koitschev A, Kusnyerik A, Sachs H, Schatz A, Stingl K, Peters T, Wilhelm B, Zrenner E. Artificial vision with wirelessly powered subretinal electronic implant alpha-IMS. *Proc Biol Sci* 280: 20130077, 2013.

Tian M, Jarsky T, Murphy GJ, Rieke F, Singer JH. Voltage-gated Na channels in AII amacrine cells accelerate scotopic light responses mediated by the rod bipolar cell pathway. *J Neurosci* 30: 4650–4659, 2010.

Toychiev AH, Ivanova E, Yee CW, Sagdullaev BT. Block of gap junctions eliminates aberrant activity and restores light responses during retinal degeneration. *J Neurosci* 33: 13972–13977, 2013.

Trenholm S, Borowska J, Zhang J, Hoggarth A, Johnson K, Barnes S, Lewis T, Awatramani G. Intrinsic oscillatory activity arising within the electrically-coupled AII amacrine/ON cone bipolar cell network is driven by voltage-gated Na^+ channels. *J Physiol* 590: 2501–2517, 2012.

Veruki ML, Hartveit E. Electrical synapses mediate signal transmission in the rod pathway of the mammalian retina. *J Neurosci* 22: 10558–10566, 2002.

Wu SN, Hsu MC, Liao YK, Wu FT, Jong YJ, Lo YC. Evidence for inhibitory effects of flupirtine, a centrally acting analgesic, on delayed rectifier K^+ currents in motor neuron-like cells. *Evid Based Complement Alternat Med* 2012: 148403, 2012.

Ye JH, Goo YS. The slow wave component of retinal activity in rd/rd mice recorded with a multi-electrode array. *Physiol Meas* 28: 1079–1088, 2007.

Yee CW, Toychiev AH, Sagdullaev BT. Network deficiency exacerbates impairment in a mouse model of retinal degeneration. *Front Syst Neurosci* 6: 8, 2012.

Zenisek D, Matthews G. Calcium action potentials in retinal bipolar neurons. *Vis Neurosci* 15: 69–75, 1998.